JOURNAL OF MAGNETIC RESONANCE, Series A **120,** 46–55 (1996)
ARTICLE NO. 0098

^{15}N Chemical-Shift Tensors and Hydrogen-Bond Geometries of 3,5-Substituted Pyrazoles and Their Orientation in the Molecular Frame

C. G. HOELGER,* F. AGUILAR-PARRILLA,* J. ELGUERO,† O. WEINTRAUB,‡ S. VEGA,‡ AND H. H. LIMBACH*

*Institut für Organische Chemie, Freie Universität Berlin, Takustr. 3, 14195 Berlin, Federal Republic of Germany; †Instituto de Química Médica, C.S.I.C., Juan de la Cierva, 28006 Madrid, Spain; and ‡Chemical Physics Department, Weizmann Institute of Science, 76100 Rehovot, Israel

Received October 30, 1995

The results of various ^{15}N solid-state NMR experiments performed on solid samples of doubly ^{15}N-labeled 3,5-dimethylpyrazole, 5-methyl-3-phenylpyrazole, (PMP), and 3,5-diphenylpyrazole are reported. In the solid state, these compounds form various hydrogen-bonded complexes. The principal values of the ^{15}N chemical-shift tensors (CST) of amine and imine nitrogen atoms are derived by lineshape analysis of the ^{15}N NMR spectra of the static powders obtained under the conditions of ^{1}H–^{15}N cross polarization and ^{1}H decoupling. The orientations of the ^{15}N CST in the molecular principal axis system are obtained by taking into account the ^{15}N–^{15}N dipolar interactions and the ^{15}N–D dipolar interaction after deuteration of the mobile proton sites. The relative orientations of the amine and imine CST in PMP are independently checked by one-dimensional off-magic axis sample spinning magnetization transfer experiments. The isotropic chemical shifts, the principal elements, and the orientations of the CST of both nitrogen atoms and the ND distances depend only slightly on the chemical structure and the associated hydrogen-bonded structure. The intramolecular structure of pyrazoles, therefore, does not vary substantially when different types of hydrogen-bonded complexes are formed.

INTRODUCTION

One of the most important measurable quantity of nuclear magnetic resonance spectroscopy is the isotropic chemical shift, which allows the discrimination of signals of various chemical structures, conformations, and environments and their empirical assignment. In compounds containing hydrogen bonds involving nitrogen, the ^{15}N isotropic chemical shift provides valuable information on the structure and the proton dynamics of N–H · · · X hydrogen bonds in the liquid state, as well as the solid state (*1–3*). The chemical shielding, however, depends on the orientation of the molecule with respect to the external magnetic field and is described by the three principal elements of the chemical-shift tensor (CST). This orientation dependence is particularly important for the investigation of solids, where the molecules are more or less rigid and no motional averaging occurs. The information on the size of the CST and its orientation in the molecular principal axis system (PAS) is necessary for the analysis of several solid-state NMR experiments, e.g., for distance measurements by dipolar couplings in static powder spectra (*4*), by rotational resonance experiments (*5*) or multipulse techniques (*6*), for the evaluation of structures by CST correlation (*7*), for the detection of molecular motions (*8*), or for the analysis of relaxation phenomena (*9*). The size of the three principal elements of the CST can provide additional information, which is empirically interpreted and becomes more important with an increasing number of data available (*10*).

In the present paper, we report our investigation of ^{15}N CST in 3,5-dimethylpyrazole (DMP), β-5-methyl-3-phenylpyrazole (β-PMP), and 3,5-diphenylpyrazole (DPP) (Fig. 1). Our interest in these compounds actually stems from the study of their solid-state hydrogen bonding and proton tautomerism. The chemical structure variations of these compounds leads to interesting differences in the solid-state hydrogen-bonded structure: DMP forms cyclic trimers and DPP cyclic tetramers in which degenerate triple and quadruple proton transfers take place as shown by ^{15}N CPMAS experiments (MAS = magic-angle sample spinning) (*11*). The rate constants of these processes depend strongly on temperature. PMP exhibits polymorphism (*12*). α-PMP crystallizes from hydrocarbons and forms cyclic tetramers (*13*) in which a degenerate quadruple proton transfer takes place according to Fig. 1c, as in solid DPP. By contrast, β-PMP is obtained from methanol by evaporation and does not exhibit a solid-state proton tautomerism; i.e., only one tautomer is formed. Its X-ray crystallographic structure is not yet known (*13*). The modification studied previously (*6*) and in this study refers to β-PMP.

Since one can expect the proton tautomerism to affect the CST of both types of pyrazole nitrogen atom sites, we had to study these compounds under the conditions where the protons are localized, i.e., DMP and DPP at low temperatures and β-DPP at room temperature. Generally, the elements were derived by lineshape analysis of the ^{15}N static powder spectra of the doubly ^{15}N-labeled compounds, protonated and deuterated in the mobile proton sites. Thus, the observa-

1064-1858/96 $18.00

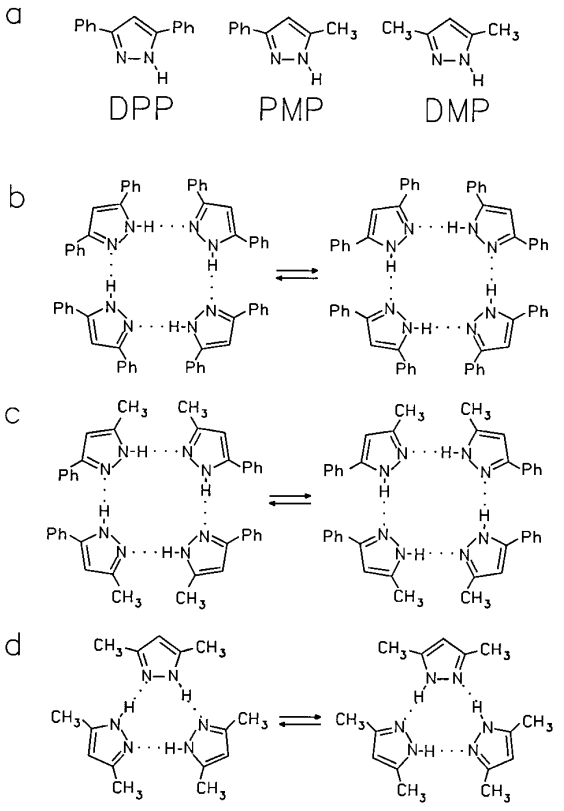

FIG. 1. (a) Chemical structure of 3,5-diphenylpyrazole (DPP), 5-methyl-3-phenylpyrazole (PMP), and 3,5-dimethylpyrazole (DMP). The protonated nitrogen atoms (–NH–) are also labeled ''amino'' and the nonprotonated nitrogen atoms (=N—) as ''imino'' nitrogen atoms. (b) Degenerate quadruple proton transfer in cyclic tetramers of crystalline DPP according to Ref. (*12c*). (c) Degenerate quadruple proton transfer in cyclic tetramers of crystalline α-PMP according to Ref. (*13*). The structure of β-PMP where the protons are ordered, i.e., localized, (*13*) is not known. (d) Degenerate quadruple proton transfer in cyclic trimers of crystalline DMP according to Ref. (*12*).

tion of the ^{15}N–^{15}N dipolar couplings as well as the ^{15}N–D dipolar couplings (*14*) allowed us to determine the orientation of the CST of the two pyrazole nitrogen sites with respect to the molecular PAS, i.e., the internuclear vectors. The relative orientations of the CST could also be determined in the case of DMP and DPP at elevated temperatures where the degenerate proton transfer averages both tensors. Data concerning the size and orientation of CST are still scarce. In addition, from the ^{15}N–D dipolar couplings, the distances between nitrogen and the adjactant deuterium in the hydrogen bonds of the different compounds could be obtained.

In order to check the results inferred from the static powder spectra, one-dimensional off-magic axis spinning magnetization transfer (OMAS MT) experiments were performed. Magnetization transfer between the orientation-dependent signals of powder spectra allows the determination of the relative orientations of CST of neighboring spins through spin diffusion or spins in different states through molecular motions or chemical exchange. Valuable information about structures and molecular reorientations has thus been obtained by two-dimensional magnetization-transfer experiments (*7, 8*). Here, we use the one-dimensional technique to obtain the relative orientation of the CST of amine and imine nitrogen atoms, which can be compared with the results inferred from the lineshape analysis of the static powder spectra.

EXPERIMENTAL

Doubly ^{15}N-labeled pyrazoles DMP, PMP, and DPP were prepared as described in Ref. (*15*) with $^{15}N_2$-enriched hydrazine sulfate (95% ^{15}N). NMR measurements at 2.1 T were performed on a Bruker CXP 100 NMR spectrometer equipped with a superconducting magnet. A 7 mm standard probehead from Doty Scientific Instruments was employed. Measurements at 7 T were performed with a Bruker MSL 300 equipped with a 5 mm probehead. Variable temperature NMR was performed using a homebuilt heat exchanger (*16*). All spectra are referenced to external solid $^{15}NH_4Cl$. The angles in OMAS experiments were determined by simulation of a spectrum of $NH_4{}^{15}NO_3$ with the parameter σ_{11} = 191 ppm, σ_{22} = 390 ppm, and σ_{33} = 421 ppm. Calculations of the spectra were carried out on a personal computer with a program based on the equations given in the following section, taking into account 1000–4000 different orientations described by the angles Θ and Φ and for OMAS spectra, the average being over 30 values for Ψ. Errors were calculated according to Ref. (*17*).

GENERAL SECTION

Calculation of Static and OMAS Powder Spectra

The principles for the calculations of powder patterns of S spins, which consider chemical-shift interaction and heteronuclear dipolar couplings to I spins as well as homonuclear couplings, have been published previously (*4, 10a, 14*) and will be repeated here briefly for convenience.

The resonance frequency ν^S of spins S embedded in a static powder in absence of homonuclear couplings depends on their orientation with respect to the external magnetic field described by the angles θ and ϕ and is given by

$$\nu^S(\theta, \phi) = \nu^S_{zee} + \nu^S_{cs} + \sum_I m_I \nu^{SI}_d. \qquad [1]$$

As usual, $\nu_{zee} = \gamma_S B_0/2\pi$ represents the Zeeman interaction of S, ν^S_{cs} the chemical-shift anisotropy, and ν^{SI}_d the contribution arising from dipolar coupling of S with spin I. ν^S_{cs} is given in the usual secular approximation by

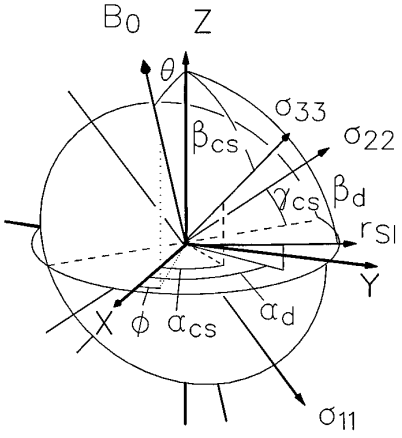

FIG. 2. Definition of angles α_{cs}, β_{cs}, γ_{cs} and α_d, β_d for the orientation of the chemical-shift tensor and internuclear vector in an arbitrary principal axis system.

$$\nu_{cs}^{S} = (\gamma_S B_0/2\pi) \times (\sigma_{11}^{S}\cos^2\theta_{11}^{S} + \sigma_{22}^{S}\cos^2\theta_{22}^{S} + \sigma_{33}^{S}\cos^2\theta_{33}^{S}), \quad [2]$$

where θ_{ii}^{S} is the angle between B_o and σ_{ii}^{S}; the contributions of the dipolar S–I coupling are given by

$$\nu_d^{SI} = D_{SI}\{1 - 3\cos^2\theta_d^{SI}\}, \quad [3]$$

$$D_{SI} = (\gamma_S\gamma_I h\mu_0/16\pi^3)/r_{SI}^3. \quad [4]$$

D_{SI} is the dipolar coupling constant, θ_d^{SI} is the angle between the SI vector and the magnetic field, γ_S and γ_I are the gyromagnetic ratios, μ_0 is the permeability, and h is Planck's constant.

As illustrated in Fig. 2, in a molecular frame of reference with the coordinates X, Y, Z, the orientation of the magnetic field vector B_o is related to this frame by the angles θ and ϕ. The orientation of the distance vector r_{SI} between S and I is given by the angles α_d and β_d. The orientation of the principle components of the CST is given by the Euler angles α_{cs}, β_{cs}, and γ_{cs}. If all angles are zero, $\sigma_{11}\|X$, $\sigma_{22}\|Y$, and $\sigma_{33}\|Z$. Any arbitrary orientation is then obtained as usual by three consecutive positive rotations, i.e., α_{cs} about σ_{11}, β_{cs} about σ_{22}, and γ_{cs} about σ_{11}. On inspection of Fig. 2, it follows by common geometric arguments that

$$\cos\theta_{11}^{S} = \cos\gamma_{cs}^{S}\cos\beta_{cs}^{S}\sin\theta\cos(\phi - \alpha_{cs}^{S}) + \sin\gamma_{cs}^{S}\sin(\phi - \alpha_{cs}^{S}) - \cos\gamma_{cs}^{S}\sin\beta_{cs}^{S}\cos\theta, \quad [5]$$

$$\cos\theta_{22}^{S} = -\sin\gamma_{cs}^{S}\cos\beta_{cs}^{S}\sin\theta\cos(\phi - \alpha_{cs}^{S}) + \cos\gamma_{cs}^{S}\sin(\phi - \alpha_{cs}^{S}) + \sin\gamma_{cs}^{S}\sin\beta_{cs}^{S}\cos\theta, \quad [6]$$

$$\cos\theta_{33}^{S} = \sin\beta_{cs}^{S}\sin\theta\cos(\phi - \alpha_{cs}^{S}) + \cos\beta_{cs}^{S}\cos\theta. \quad [7]$$

From Fig. 2, it follows that $\cos\theta_d^{SI}$ is given by

$$\cos\theta_d^{SI} = \sin\beta_d^{SI}\sin\theta\cos(\phi - \alpha_d^{SI}) + \cos\beta_d^{SI}\cos\theta. \quad [8]$$

In the presence of a fast dynamic exchange between different states j, the resulting frequency is simply obtained by

$$\nu^{S}(\theta, \phi) = \sum_j p(j)\nu^{S}(j, \theta, \phi), \quad [9]$$

where $\nu^{S}(j, \theta, \phi)$ is the absorption frequency and $p(j)$ is the probability of state j.

In order to calculate spectra under sample spinning conditions, the molecular PAS is defined in the rotor-axis frame by the Euler angles Ψ, Θ, and Φ. θ and ϕ are then given by

$$\theta = \arccos z, \quad [10]$$

$$\phi = \arccos[x/(1 - z^2)^{0.5}], \quad [11]$$

where

$$z = -\sin\Theta\cos\Psi\sin\Omega + \cos\Theta\cos\Omega, \quad [12]$$

$$x = -\cos\Phi\cos\Theta\cos\Psi\sin\Omega - \cos\Phi\sin\Theta\cos\Omega - \sin\Phi\sin\Psi\sin\Theta. \quad [13]$$

Ω is the magic angle between the rotor axis and the direction of the magnetic field, Ψ describes the rotation of the sample around the rotor axis, Θ is the angle between the Z component of the PAS and the rotor axis, and Φ defines the final rotation of the molecule around the Z component of the PAS. The spinning averaged frequencies $\bar{\nu}^{S}(\Omega, \Theta, \Phi, m_I)$ are then obtained by

$$\bar{\nu}^{S}(\Omega, \Theta, \Phi, m_I) = 1/2\pi \int_0^{2\pi} \nu^{S}(\Omega, \Psi, \Theta, \Phi, m_I)d\Psi, \quad [14]$$

which is numerically calculated.

The powder spectrum of S is obtained by calculating $\nu^{S}(\Theta, \Phi)$ in increments for Θ and Φ. The corresponding signal intensities of a certain orientation $M(\Omega, \Theta, \Phi)$ are given by their probability; i.e., the value of $\sin\Theta$ and are convoluted with a line-broadening function.

Calculation of Homonuclear Dipolar Couplings

The calculation of ^{15}N powder spectra of doubly ^{15}N-labeled pyrazoles requires the considerations of the homonuclear character of the dipolar interaction between the two nitrogen atoms (*4a, 10a*). As a consequence, the position and the intensity of the signals of homonuclear spins S = A, B depend on the ratio between the homonuclear dipolar interaction and the difference $\delta\nu$

$$\delta\nu = \bar{\nu}^{A}(\Omega, \Theta, \Phi, m_{I}) - \bar{\nu}^{B}(\Omega, \Theta, \Phi, m_{I}), \quad [15]$$

a result which somehow resembles the well-known AB case of *J*-coupled spins in high-resolution NMR spectra. It is convenient to define the quantities P, Q, and R as

$$P = 1/2[\bar{\nu}^{A}(\Omega, \Theta, \Phi, m_{I^a}) + \bar{\nu}^{B}(\Omega, \Theta, \Phi, m_{I^b})], \quad [16]$$

$$Q = 1/4D_{AB}[1 - 3(\cos^2\beta_{d}^{AB}\sin\theta\cos(\phi - \alpha_{d}^{AB}) + \cos\beta_{d}^{AB}\cos\theta)^2], \quad [17]$$

$$R = \left(Q^2 + \frac{\delta\nu^2}{4}\right)^{1/2}. \quad [18]$$

The four transition frequencies and corresponding intensities of the homonuclear dipolar coupled two-spin system is then given by

$$\nu_1(\Omega, \Theta, \Phi, m_{I^a}, m_{I^b}) = P + 2Q - R,$$
$$M_1(\Omega, \Theta, \Phi, m_{I^a}, m_{I^b}) = \left(1 - \frac{Q}{R}\right)\sin\Theta \quad [19]$$

$$\nu_2(\Omega, \Theta, \Phi, m_{I^a}, m_{I^b}) = P - 2Q - R,$$
$$M_2(\Omega, \Theta, \Phi, m_{I^a}, m_{I^b}) = \left(1 + \frac{Q}{R}\right)\sin\Theta \quad [20]$$

$$\nu_3(\Omega, \Theta, \Phi, m_{I^a}, m_{I^b}) = P + 2Q + R,$$
$$M_3(\Omega, \Theta, \Phi, m_{I^a}, m_{I^b}) = \left(1 + \frac{Q}{R}\right)\sin\Theta \quad [21]$$

$$\nu_4(\Omega, \Theta, \Phi, m_{I^a}, m_{I^b}) = P - 2Q + R,$$
$$M_4(\Omega, \Theta, \Phi, m_{I^a}, m_{I^b}) = \left(1 - \frac{Q}{R}\right)\sin\Theta. \quad [22]$$

Because of mixed terms in the wave functions, these transitions can no longer be assigned to spin A or B alone.

Calculation of OMAS Magnetization Transfer Spectra

Magnetization transfer in or between orientation-dependent signal patterns, arising either from homonuclear spectral spin diffusion between nearby nuclei or from chemical exchange, allows the determination of the relative orientation of the CST of various nuclear sites. However, the method is only satisfactory if the spectral contributions of the CST of the different sites can be separated, a condition which is generally not achieved for static powders containing nuclei in different chemical sites. If the sample contains only a few sites with substantially different isotropic chemical shifts, as often realized in the case of ^{15}N NMR of ^{15}N-labeled compounds, off-magic-angle sample spinning (OMAS) about an axis forming the angle Ω with the magnetic field may be helpful, and scales the effective CST elements in such a way that well-separated powder patterns for each individual line can be observed. In this case, magnetization transfer between the sites via slow chemical exchange or spectral spin diffusion is of assistance when determining the relative orientations of the various CST.

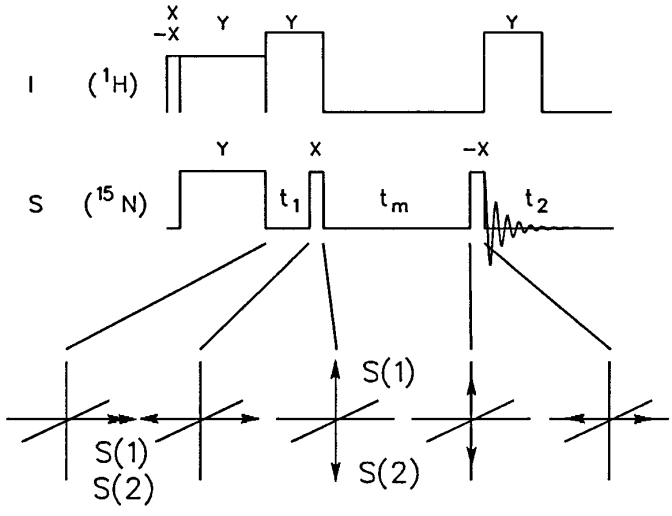

FIG. 3. Pulse sequence of magnetization transfer experiment.

The basic pulse sequence employed in this study under static or OMAS conditions is illustrated in Fig. 3. This sequence has been probed in many one-dimensional MAS MT experiments with a few values of the evolution time t_1 (*18*) as well as in two-dimensional experiments (*7, 8*) involving sampling for a set of t_1 values and Fourier transformation. The cross-polarization transverse magnetization along the *y* direction of the rotation frame of reference characterized by the frequency ν^{ref} evolves in t_1 with the frequency $\nu^{S}(\Omega, \Theta, \Phi)$. At t_1, the transverse magnetization is converted into longitudinal magnetization

$$M^{S}(t_1, \Omega, \Theta, \Phi) = \cos[2\pi(\nu^{ref} - \bar{\nu}^{S}(\Omega, \Theta, \Phi, m_{I})t_1]\sin\Theta \quad [23]$$

by a 90°_{x} pulse evolving during the mixing time t_m which is generally long in comparison to the transverse relaxation time. Therefore, remaining transverse magnetization is rap-

TABLE 1
NMR Parameters of Solid DPP, DMP, and PMP Obtained in This Study by Solid-State ^{15}N NMR

	Type	σ_{11}	σ_{22}	σ_{33}	σ_{iso} [a]	α_{CS}	β_{CS}	γ_{CS}	r_d^{NN}	r_d^{ND}	α_d^{ND}	β_d^{ND}
DPP	–NH–	242 ± 3	180 ± 3	66 ± 3	163 (163)	120 ± 2	1 ± 4	0	1.345 ± 0.015	1.052 ± 0.003	123 ± 2	90 ± 2
β-PMP	–NH–	267 ± 3	165 ± 2	69 ± 2	167 (167)	131 ± 2	0 ± 6	0	1.345 ± 0.015	1.044 ± 0.003	128 ± 2	90 ± 2
DMP	–NH–	254 ± 3	175 ± 3	72 ± 3	167 (167)	126 ± 3	0 ± 4	0	1.340 ± 0.015	1.042 ± 0.003	118 ± 4	90 ± 3
	Type	σ_{11}	σ_{22}	σ_{33}	σ_{iso} [a]	α_{CS}	β_{CS}	γ_{CS}	r_d^{NN}	$r_d^{ND'}$	$\alpha_d^{ND'}$	$\beta_d^{ND'}$
DPP	–N=	410 ± 2	254 ± 4	46 ± 2	237 (236)	−20 ± 2	2 ± 6	0	1.345 ± 0.015	1.85 ± 0.04	70 ± 5	90 ± 6
β-PMP	–N=	409 ± 3	257 ± 4	39 ± 2	236 (235)	−21 ± 2	0 ± 3	0	1.345 ± 0.015	1.93 ± 0.03	70 ± 6	92 ± 8
DMP	–N=	399 ± 3	258 ± 4	70 ± 3	242 (241)	−16 ± 2	0 ± 6	0	1.340 ± 0.015	1.84 ± 0.04	73 ± 5	90 ± 6

Note. α_{iso}, isotropic ^{15}N chemical shifts of the amino (–NH–) and imino (–N=) nitrogen atom sites in parts per million with respect to solid $^{15}NH_4Cl$ as reference; σ_{11}, σ_{22}, σ_{33}, elements of the corresponding chemical-shift tensors; α_{cs}, β_{cs}, γ_{cs}, Euler angles relating the chemical shift(subscript cs) tensors to a molecular, fixed principal axis system with the X axis pointing in the direction of the N . . . N bond and the Z axis perpendicular to the molecular plane; r_d^{NX}, cubic average distance between N and X (N or D) in angstroms derived from the corresponding dipolar coupling tensor where the subscript signifies "dipolar" (i.e., r_d^{NN} represents the dipolar N . . .N distance, r_d^{ND} the dipolar short N . . .D distance in the case of amino nitrogen atoms, and $r_d^{ND'}$ the long N . . . D′ distance across the hydrogen bond in the case of the imino nitrogen atoms); α_d^{NX} and β_d^{NX}, corresponding polar angles between the vector N . . . X in the principal axis system (i.e., $\alpha_d^{NN} = 0°$, $\beta_d^{NN} = 90°$ by definition).

[a] Values in parentheses from CPMAS measurements.

idly destroyed and phase cycling employed in liquid state experiments is not necessary. When t_m is long enough and MT complete, the longitudinal magnetization is distributed among neighboring nuclei and $M^S(t_1, \Omega, \Theta, \Phi)$ is given by

$$M^S(t_1, \Omega, \Theta, \Phi) = \frac{1}{n}\sum_{S=1}^{n} \cos[2\pi(\nu^{ref} - \nu^S(\Omega, \Theta, \Phi, m_I)t_1]\sin\Theta. \quad [24]$$

This quantity is then detected by conversion to transverse magnetization using a second 90°_x pulse.

RESULTS

All parameters obtained in this ^{15}N solid-state NMR study of DPP, DMP, and PMP are assembled in Table 1 and illustrated in Fig. 4. For convenience, a molecular fixed frame is used (Figs. 4a and 4b), whose X axis points in the direction of the NN axis and the Z axis in the direction perpendicular to the molecular plane. Thus, by definition, the Euler angles relate the dipolar NN coupling tensor to the molecular fixed frame (see Fig. 2) $\alpha_d^{NN} \equiv 0°$ and $\beta_d^{NN} \equiv 90°$ by definition. In a first stage of this study, we obtained the parameters of Table 1 by ^{15}N NMR lineshape analysis. In a second stage, these parameters were verified in independent ways. A detailed account of the data analysis is given in the following sections.

^{15}N Lineshape Analysis of the Static Pyrazole Powders under Conditions of Slow Proton Tautomerism

In order to demonstrate how the parameters of Table 1 were obtained by ^{15}N lineshape analysis, let us first discuss some typical superimposed experimental and calculated ^{15}N CP NMR spectra of a static powdered DPP depicted in Fig. 5. These spectra were obtained at two different magnetic field strengths, i.e., 7 and 2.1 T and at different temperatures. At low temperatures, proton tautomerism is slow with respect to the NMR time scale and the spectra in Figs. 5a, 5c, and 5e are the sum of two overlapping contributions from the amino and the imino nitrogen sites. At high field, the influence of homonuclear dipolar ^{15}N coupling is minimal and the spectra can be simulated in crude approximation by taking into account only the CST elements σ_{11}, σ_{22}, and σ_{33} of the amino and the imino nitrogen sites. The orientations of both tensors in the molecular fixed frame cannot be precisely obtained from Fig. 5a. By contrast, the low-field spectrum of Fig. 5c cannot be simulated without consideration of the homonuclear ^{15}N coupling. Therefore, by using the known CST elements, the cubic average N · · · N distance r_d^{NN} and the absolute values of the Euler angles α_{cs}, β_{cs}, and γ_{cs} connecting the two chemical-shift tensors to the molecular frame could be obtained by analysis of the lineshape of

Fig. 5c. At first, it seems unlikely that so many additional parameters could be obtained; however, because of the molecular symmetry—in particular because of the mirror plane of the pyrazole ring—we expected one tensor component to be located parallel to the Z axis, from which it follows that two Euler angles should be zero for both nitrogen sites. Thus, by lineshape analysis of Fig. 5c, (i) the value of r_d^{NN} was determined, (ii) it followed that σ_{33} pointed into the Z direction as illustrated in Fig. 4a, i.e., that β_{cs} and γ_{cs} were close to zero for both nitrogen sites, and (iii) the absolute values of α_{cs} for both nitrogen sites was derived. In order to determine the signs of α_{cs}, we measured the spectrum of the monodeuterated compound DPP-d_1 at low temperatures and 2.1 T depicted in Fig. 5e. In comparison with Fig. 5c, the influence or the dipolar ND coupling becomes evident.

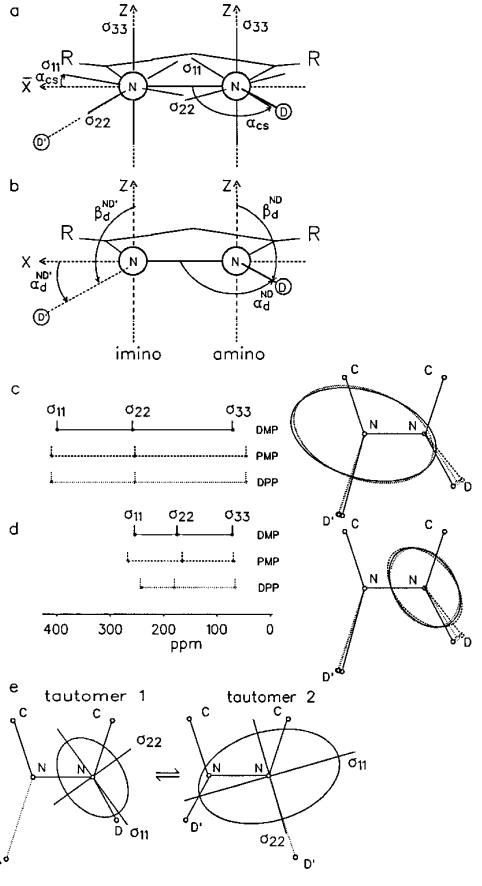

FIG. 4. Results of the ^{15}N solid-state NMR measurements performed on solid pyrazoles obtained in this study. (a) Orientation of ^{15}N chemical-shift tensors of the amino and the imino nitrogen atom sites of DPP and in good approximation for β-PMP and DMP in the molecular frame. (b) Orientation of the dipolar N–D coupling tensor in the molecular frame. (c) and (d) Representation of principal values of ^{15}N chemical-shift tensors of the imino and the amino nitrogen atom sites in DPP, PMP, and DMP. Reference: solid $^{15}NH_4Cl$. The ellipses represent the tensor elements σ_{11} and σ_{22} for the long and short axes, both located in the molecular pyrazole plane. (e) Change of the ^{15}N chemical-shift tensor of DPP during tautomerism.

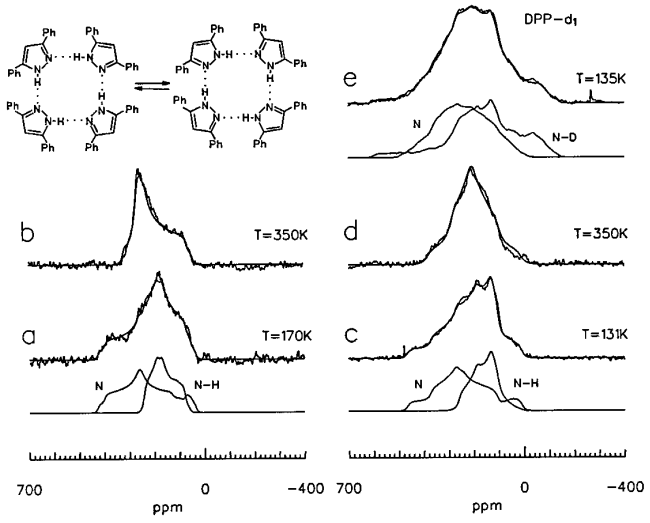

FIG. 5. Superimposed experimental and calculated ^{1}H-decoupled ^{15}N static powder spectra of doubly ^{15}N-labeled DPP and its mono-deuterated isotopomer DPP-d_1 under various experimental conditions. Reference: solid $^{15}NH_4Cl$. (a, b) DPP, 7 T (30.41 MHz), (c, d) DPP, 2.1 T (9.12 MHz); (e, f) DPP-d_1, 2.1 T (9.12 MHz). In (a, c, e), the calculated subspectra of the amino and the imino nitrogen sites are presented. The site intensities were calculated according to the square of the coefficients in the mixed wave functions.

Through lineshape analysis of this spectrum, information was obtained about (i) the values of the short nitrogen–deuteron distance r_d^{ND} for the amino site, (ii) the long distance $r_d^{ND'}$ for the imino site, (iii) the corresponding Euler angles α_d^{ND} and $\alpha_d^{ND'}$ defined in Fig. 4b, and (iv) the absolute signs of α_{cs} for both nitrogen sites, taking into account that the Euler angles β_d^{ND} and $\beta_d^{ND'}$ are zero because of the molecular symmetry.

For the lineshape analysis of the DMP spectra at low temperatures, we proceeded in the same way, as also for the room temperature spectra of β-PMP, which is not affected by proton tautomerism. The results obtained are compared in Figs. 4c and 4d. In this manner, the remaining parameters of Table 1 were determined.

Confirmation of the Analysis for DPP and DMP by Lineshape Analysis of the ^{15}N Spectra in the Regime of Fast Proton Tautomerism

The ^{15}N spectra of DPP and DMP taken at elevated temperatures show important changes as compared to the low-temperature spectra as demonstrated for DPP in Figs. 5b, 5d, and 5f. From the analysis of the corresponding ^{15}N CPMAS spectra (*11*), it was known that these spectral changes arise from fast, degenerate, solid-state proton tautomerism. The difference between amino and imino nitrogen sites is, however, no longer justified and the spectra consist only of the contribution of a single nitrogen site, because the degeneracy of the tautomerism implies the formation of two equally

populated tautomers. Due to this degeneracy, it was natural to assume that the tautomers are enantiomers related by a mirror symmetry as in the gas phase. The change of the ^{15}N CST and the dipolar ND coupling tensors during the proton transfer can thus be obtained from the tensors of the neighboring nitrogen atom site by simple symmetry arguments as illustrated in Fig. 4e. If this assumption is true, it should be possible to simulate the high-temperature ^{15}N CP NMR spectra of DPP and DMP using the parameters of Table 1. Moreover, a good agreement between the calculated and the experimental spectra would corroborate the Euler angles of Table 1.

In fact, as illustrated in Figs. 5d and 5f, the agreement was very satisfactory. Furthermore, the simulation of the high-field spectrum of Fig. 5b in terms of only the components of the CSTs and the Euler angles relating the two tensors calculated from Table 1 also led to a satisfactory result. The parameters of Table 1 could therefore be corroborated for DPP and also in a similar way for DMP.

Confirmation of the Analysis for β-DPP by One-Dimensional Off-Magic-Angle Magnetization Transfer (OMAS MT) via Homonuclear Spectral ^{15}N Spin Diffusion

In the case of β-PMP, the proton tautomerism is, as mentioned above, suppressed and a different strategem was applied in order to corroborate the results of the lineshape analyses. We performed OMAS MT experiments on PMP, taking advantage of the spectral spin diffusion between the adjacent ^{15}N atoms of the doubly labeled compound. Figure 6a shows the 7 T OMAS spectrum of PMP where the angle of the rotation axis and the magnetic field was $\Omega = 65.3°$. This spectrum corresponds to a value of $t_1 = 0$ s in the pulse sequence of Fig. 3. In contrast to the spectrum of the static powder which looks similar to the DPP spectrum of Fig. 5a, the two contributions of the amino and the imino nitrogen sites are fairly now well separated. Therefore, the small effects of the dipolar homonuclear ^{15}N coupling can be taken into account in good approximation using the simpler theory of heteronuclear dipolar coupling expressed in Eqs. [1]–[4]. Figures 6b and 6d depict the OMAS spectra after two different times t_1 and a mixing time of $t_m = 10$ ms. This time was too short to allow an effective magnetization transfer by spin diffusion. In contrast, the spectra in Figs. 6c and 6e are obtained by a mixing time of $t_m = 10$ s, leading to substantial lineshape changes caused by magnetization transfer via spin diffusion between the adjacent ^{15}N spins. The agreement with the experimental and the calculated spectra is very satisfactory. The agreement was achieved mainly by varying the angles relating the amino and the imino CST. The parameters obtained coincided within the margin of error with those assembled in Table 1, confirming in an independent way, the results obtained by lineshape analysis of the spectra of the static powders.

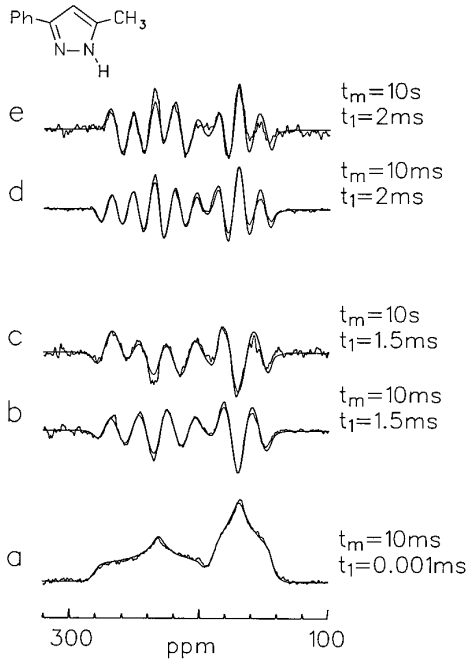

FIG. 6. Superimposed experimental and calculated ^{1}H-decoupled ^{15}N off-magic-angle spinning (OMAS) NMR spectra of $^{15}N_2$-PMP obtained at 30.41 MHz as a result of the magnetization transfer pulse sequence depicted in Fig. 3. The correlation of the amino- and imino-^{15}N chemical-shift tensors is obtained by lineshape analysis. Reference: solid $^{15}NH_4Cl$. (a) Normal OMAS spectrum with $t_1 = 1\ \mu s \approx 0$. (b)–(e) OMAS magnetization transfer spectra with $t_1 = 1.5$ ms and variable delays t_m. The parameters of the lineshape analyses are included in Table 1.

DISCUSSION

In the previous section, we reported the ^{15}N CST and the NN and ND dipolar coupling tensors of the amino (–NH–) and the imino (=N–) nitrogen sites of three solid doubly ^{15}N-labeled pyrazoles DPP, DMP, and PMP (see Figs. 1 and 4, and Table 1). The CST elements were determined mainly by analysis of the static powder spectra obtained under proton decoupling. In order to orient the amino and imino CSTs in the molecular frame of reference, advantage was taken of homonuclear dipolar ^{15}N and heteronuclear ^{15}ND coupling. The assignment was corroborated in the case of DPP and DMP by lineshape analysis of the spectra at high temperature where a fast degenerate proton tautomerism averages the spectral parameters of the amino and the imino sites. In the case of PMP where the tautomerism is suppressed, the relative orientations of the CSTs were corroborated via one-dimensional OMAS-MT experiments where the magnetization transfer is caused by spectral spin diffusion between the two adjacent ^{15}N nuclei. In general, the information was obtained by lineshape analysis of one-dimensional spectra at different evolution times as depicted in Fig. 6. Previously, such information has been determined by two-dimensional experiments (*7*), but the results presented here indicate that

TABLE 2
Crystal Geometric Data Concerning DPP, α-PMP, and DMP

			Amino nitrogen		Imino nitrogen	
	r^{NN}	$r^{N\cdots N}$	r^{NH}	α^{NH}	r^{NH}	α^{NH}
DPP[a]	1.346	2.874	1.018	125.5	1.898	—
			1.118		1.741	
DPP[b]	1.360	2.865	(1.450)	—	(1.450)	—
α-PMP[c]	1.364	2.863	(1.427)	119.5	(1.427)	119.5
DMP[d]	1.334	2.899	0.88	125.1	2.12	—
DMP[e]	1.362	2.890	0.95	124.0	1.94	—

Note. r^{NN}, intramolecular N . . .N distance; $r^{N\cdots N}$, intermolecular N . . . N distance; r^{NH}, covalent distance N–H in the case of amino nitrogen and long N . . . H distance across the hydrogen bond in the case of imino nitrogens; α^{NH}, angle between the NH vector and the NN vector.

[a] Reference (*12*).

[b] Reference (*23*).

[c] Reference (*13*).

[d] (Room temperature): Refs. (*11, 24*).

[e] At −146°C, Ref. (*25*).

in the case of few molecular sites as is generally realized in ^{15}N NMR, one-dimensional experiments are also helpful. Such experiments have the advantage in that they are less time consuming than two-dimensional experiments and that lineshape analysis from which quantitative information can be obtained is easier.

In the remainder of this section, we discuss the parameters obtained in context to selected crystallographic parameters assembled in Table 2. There are significant differences in the type of parameters obtained by NMR and X-ray crystallography. By low-temperature NMR, only the intramolecular pyrazole structure is observed involving localized protons. At room temperature, a fast degenerate proton tautomerism is observed for DPP and DMP, i.e., dynamic proton disorder. By contrast, in X-ray crystallography, both the intramolecular or primary structure and the secondary and the tertiary hydrogen-bonded structures are observed and averaged over all tautomeric states. Furthermore, the bond lengths obtained by NMR are cubic averages which are generally shorter than the average distances obtained by X-ray crystallography. A further complication is that the bond lengths determined by NMR may be affected by small angle reorientation of the distance vectors in space arising from molecular mobilities, eventually leading to a reduced dipolar coupling and hence to distances which are larger than those obtained by crystallography.

Let us first discuss the outcome of the chemical-shift anisotropy determinations. The principal elements of ^{15}N CST in DPP, β-PMP, and DMP assembled in Table 1 were visualized in Fig. 4. Only small variations between the different compounds are observed (Figs. 4c and 4d). For the amino (–NH–) sites, the most shielded component σ_{33} of the CST is more or less similar and located perpendicular to the pyrazole ring. Small differences appear in both σ_{11} and σ_{22} which are located in the plane of the pyrazole ring along the main directions of the ellipses depicted in Figs. 4c and 4d, σ_{11} being almost parallel to the ND vector. For the nonprotonated imino nitrogen sites, σ_{33} is again located perpendicular to the molecular plane and is similar for the amino nitrogen sites. However, σ_{11} and σ_{22} are strongly deshielded leading to a low-field isotropic chemical shift which can be understood in terms of a paramagnetic deshielding associated with a low-energy n → π^* transition. Figure 4e illustrates the change of the chemical-shift tensor of the amino nitrogen site when the proton transfer occurs, i.e., when the site is converted into an imino site. The shielding in the directions parallel to the hydrogen bond and perpendicular to the pyrazole ring is almost identical, and the difference of about 70 ppm in the isotropic chemical shifts of the amino and the imino nitrogen sites therefore arises from the deshielding in the direction of σ_{11} of the imino site. In conclusion, the ^{15}N chemical-shift tensors of pyrazoles depend strongly on whether the nitrogen is protonated or not, but less on the chemical structure. Since small changes of the substituents lead to large changes of the secondary hydrogen-bonded structure, it follows that the CST of the compounds studied here are also not very sensitive to the latter.

This result can be explained in terms of the finding that the short dipolar ND distances r_d^{ND} between the hydrogen-bonded deuteron and the amino nitrogen in DPP, β-PMP, and DMP obtained from the analysis of the spectra of the ND-deuterated compounds are not significantly different, i.e., around 1.05 Å, despite the different secondary hydrogen-bonded structure. Also, the long distance $r_d^{ND'}$ between the deuteron and the imino nitrogen atom across the hydrogen bond, which is on the order of 1.9 Å, does not vary too much. The cubic average of both distances can be calculated from the equation

$$\frac{1}{r^3} = \frac{0.5}{(r^{ND})^3} + \frac{0.5}{(r^{ND'})^3}, \qquad [25]$$

and $\bar{r}$ is on the order of 1.25 Å. The spectrum of DPP at a high temperature where the proton transfer is fast and degenerate (Fig. 5f) could also be simulated using the single distance r. We note that this distance is shorter than expected from half of the crystallographic distance $r^{NN}/2 \cong 1.45$ Å. The finding

$$\bar{r} < r^{NN}/2 \qquad [26]$$

is not in agreement with the proton located in the center of the hydrogen bond as proposed by Fackler *et al.* (*23*), i.e., with a single-well potential, but indicates a fast tautomeric equilibrium between two forms, confirming the crystallographic structure of Ref. (*13*) (also see Table 2). In the case of DPP and DMP, this information is not absolutely necessary because the slow-exchange region could be observed at low temperatures (*13*); however, in other cases where the slow-exchange regime cannot be reached, Eq. [24] constitutes an important tool for the distinction of a single- and a double-well potential.

We observed that the hydrogen locations obtained by X-ray crystallography and NMR are not in a particularly good agreement. On the one hand, the NND angles α^{NH} which are on the order of 120° are in good agreement; on the other hand, the nitrogen–deuterium distances obtained by NMR are substantially longer than those obtained by X-ray crystallography (Table 2), which we ascribe to the known uncertainties of the latter method in establishing such distances. The NMR data, although affected by small systematic errors should be more easily comparable with neutron diffraction data which are, however, not yet available for pyrazoles. Fortunately, however, such a comparison is possible because Steiner (*19*) recently analyzed a number of published high-quality neutron diffraction data of N–H···N hydrogen bonds and observed a good correlation between the short and the long nitrogen–hydrogen distances r_1 and r_2. From Steiner's correlation, we calculate for $r_1 = 1.05$ Å an expected long distance of $r_2 = 1.77$ Å which is significantly smaller than the experimental values of $r_2 \approx 1.85$ Å listed in Table 1. On the other hand, we calculate a short distance of 1.039 Å which is closer to the experimental values. Therefore, within the margin of error, Steiner's correlation is fulfilled for solid pyrazoles. However, when making this comparison, one must keep in mind three possible complications: (i) the margins of error listed in Table 1 are purely statistical; (ii) the values determined by NMR represent cubic averages and can, therefore, be somewhat shorter than those obtained by neutron diffraction if there are large anharmonicities of the hydrogen bond vibrations, but generally, the values obtained by NMR are longer than those obtained by neutron diffraction because dipolar couplings are reduced by small angle molecular motions in the solid state (*4a*); (iii) the data obtained here by NMR refer to nitrogen–deuterium and not to nitrogen–hydrogen distances, which may be different. A systematic search in the Cambridge Structural Database (CCSD) (*21*) leads to an average N–H distance of 1.017 (±0.002) Å and an average N–D distance of 1.024 (±0.005) Å. However, these values stem from different sets of compounds and the average isotope effect may, perhaps, not be representative. We note that Lecombe and Taylor (*22*) found an increase of the nitrogen–hydrogen bond length upon deuteration of 0.006 Å for thiourea and its two modifications. By contrast, some of us recently showed by solid-state NMR a decrease of about 0.01 Å for the bond length upon deuteration for trimethylammonium salts (*14b*).

CONCLUSIONS

In conclusion, we have investigated the size and orientation of the chemical-shift tensors of amino and imino nitrogen atoms and the ND distances in three different substituted pyrazoles. The magnetization transfer in OMAS experiments should be enhanced by the application of multipulse techniques (*26*), thus increasing the potential of the method by effectively shortening the necessary mixing time required for the experiment.

ACKNOWLEDGMENTS

The assistance of Professors C. Foces-Foces (Madrid) and J. Rozière (Montpellier) is gratefully acknowledged. We thank the German–Israeli Foundation, the European Union within the framework of the Human Capital and Mobility Program ''Localization and Transfer of Hydrogen,'' and the Fonds der Chemischen Industrie Frankfurt for their support.

REFERENCES

1. (*a*) M. Witanowski, L. Stefaniak, G. A. Webb, *Annu. Rep. NMR Spectrosc.* 25, 13 (1993); (*b*) J. Elguero, N. Jagerovic, M. Foces-Foces, F. H. Cano, M. V. Roux, F. Aguilar-Parrilla, and H. H. Limbach, *Magn. Reson. Chem.* 32, 699 (1994).
2. (*a*) N. S. Golubev, S. N. Smirnow, V. A. Gindin, G. S. Denisov, H. Benedict, and H. H. Limbach, *J. Am. Chem. Soc.* 116, 12055 (1994); (*b*) R. M. Claramunt, D. Sanz, J. Catalan, F. Fabero, N. A. Garcia, M. Foces-Foces, A. L. Llamas Saiz, and J. Elguero, *J. Chem. Soc., Perkin Trans. 2,* 1687 (1993); (*c*) H. H. Limbach, *in* ''NMR Basic Principles and Progress,'' Vol. 26, Chap. 2, Springer Verlag, Berlin/New York, 1991.
3. (*a*) J. Braun, M. Schlabach, B. Wehrle, M. Köcher, E. Vogel, and H. H. Limbach, *J. Am. Chem. Soc.* 116, 6593 (1994); (*b*) E. Bär, J. Fuchs, T. Kolrep, D. Rieger, F. Aguilar-Parrilla, H. H. Limbach, and W. P. Fehlhammer, *Angew. Chem.* 103, 88 (1991); *Angew. Chem. Int. Ed.* 30, 80 (1991).
4. (*a*) K. W. Zilm and D. M. Grant, *J. Am. Chem. Soc.* 103, 2913 (1981); (*b*) R. D. Curtis, G. H. Penner, W. P. Power, and R. E. Wasylishen, *J. Phys. Chem.* 94, 4000 (1990); (*c*) R. E. Wasylishen, *Annu. Rep. NMR Spectrosc.* 23, 1 (1990).
5. D. P. Raleigh, F. Creuzet, S. K. Das Gupta, M. H. Levitt, and R. G. Griffin, *J. Am. Chem. Soc.* 111, 4502 (1989).
6. O. Weintraub, S. Vega, C. G. Hoelger, and H. H. Limbach, *J. Magn. Reson. A* 109, 14 (1994).

7. (*a*) R. Tycko and G. Dabbagh, *J. Am. Chem. Soc.* 113, 3592 (1991); (*b*) P. Robyr, B. H. Meier, and R. R. Ernst, *Chem. Phys. Lett.* 187, 471 (1991).
8. H. W. Beckham and H. W. Spiess, *in* ''NMR Basic Principles and Progress,'' Vol. 32, Chap. 4, Springer Verlag, Berlin/New York, 1994.
9. K. Anderson-Altmann and D. M. Grant, *J. Phys. Chem.* 97, 11,096 (1993).
10. (*a*) M. D. Lumsden, G. Wu, R. E. Wasylishen, and R. D. Curtis, *J. Am. Chem. Soc.* 115, 2825 (1993); (*b*) V. S. Veeman, *Prog. NMR Spectrosc.* 16, 193 (1984); (*c*) Z. Gu, R. Zambrano, and A. McDermott, *J. Am. Chem. Soc.* 116, 6368 (1994).
11. (*a*) A. Baldy, J. Elguero, R. Faure, M. Pierrot, and E. J. Vincent, *J. Am. Chem. Soc.* 107, 5290 (1985); (*b*) J. A. S. Smith, B. Wehrle, F. Aguilar-Parrilla, H. H. Limbach, M. C. Foces-Foces, F. H. Cano, J. Elguero, A. Baldy, M. Pierrot, M. M. T. Kurshid, and J. B. Larcombe-Douall, *J. Am. Chem. Soc.* 111, 7304 (1989); (*c*) F. Aguilar-Parrilla, G. Scherer, H. H. Limbach, M. Foces-Foces, F. H. Cano, J. A. S. Smith, C. Toiron, and J. Elguero, *J. Am. Chem. Soc.* 114, 9657 (1992).
12. J. Elguero, N. Jagerovic, M. Foces-Foces, F. H. Cano, M. V. Roux, F. Aguilar-Parrilla, and H. H. Limbach, *J. Heterocycl. Chem.* 32, 451 (1995).
13. (*a*) F. H. Moore, A. H. White, and A. C. Willis, *J. Chem. Soc., Perkin Trans. 2,* 1298 (1974); (*b*) E. N. Maslen, A. H. Cannon, A. H. White, and A. C. Willis, *J. Chem. Soc. Perkin Trans. 2,* 1069 (1975).
14. (*a*) Y. Hiyama, C. H. Niu, J. V. Silverton, A. Bavoso, and D. A. Torchia, *J. Am. Chem. Soc.* 110, 2378 (1988); (*b*) C. G. Hoelger and H. H. Limbach, *J. Phys. Chem.* 98, 11803 (1994).
15. R. Fusco, ''Pyrazoles, Pyrazolines, Imidazoles and Condensed Rings,'' Interscience, New York, 1967.
16. R. Kendrick, S. Friedrich, B. Wehrle, H. H. Limbach, and C. S. Yannoni, *J. Magn. Reson.* 65, 159 (1985).
17. D. W. Aldermann, M. S. Solum, and D. M. Grant, *J. Chem. Phys.* 84, 3717 (1986).
18. H. H. Limbach, B. Wehrle, M. Schlabach, R. Kendrick, and C. S. Yannoni, *J. Magn. Reson.* 77, 84 (1988).
19. T. Steiner, *J. Chem. Commun.* 1331 (1995).
20. M. D. Joesten and L. J. Schaad, ''Hydrogen Bonding,'' p. 182, Dekker, New York, 1974.
21. F. H. Allen, J. E. Davies, J. J. Galloy, O. Johnson, O. Kennard, C. F. Macrae, E. M. Mitchell, G. F. Mitchell, J. M. Smith, and D. G. Watson, *J. Chem. Inf. Comput. Sci.* 31, 187 (1991).
22. M. M. Lecombe and J. C. Taylor, *Acta Crystallogr. A* 24, 410 (1968).
23. R. G. Raptis, R. J. Staples, C. King, and J. P. Fackler, *Acta Crystallogr. C* 49, 1716 (1993).
24. A. L. Llamas-Saiz, C. Foces-Foces, F. H. Cano, P. Jiménez, J. Laynez, W. Metermans, J. Elguero, H. H. Limbach, and F. Aguilar-Parrilla, *Acta Crystallogr. B* 50, 746 (1994).
25. J. Rozière (University of Montpellier, France), personal communication.
26. (*a*) O. Weintraub, S. Vega, C. G. Hoelger, and H. H. Limbach, *J. Magn. Reson. A* 110, 12 (1994); (*b*) D. K. Sodickson, M. H. Levitt, S. Vega, and R. G. Griffin, *J. Chem. Phys.* 98, 6742 (1993); (*c*) A. E. Benett, J. H. Ok, S. Vega, and R. G. Griffin, *J. Chem. Phys.* 96, 8642 (1992); (*d*) M. Tomaselli, B. H. Meier, M. Baldus, J. Eisenegger, and R. R. Ernst, *Chem. Phys. Lett.* 225, 131 (1995).